CHIN. PHYS. LETT. Vol. 35, No. 11 (2018) 114302

Analysis of Second-Harmonic Generation of Low-Frequency Dilatational Lamb Waves in a Two-Layered Composite Plate *

Han Chen(陈瀚)[1], Ming-Xi Deng(邓明晰)[2**], Ning Hu(胡宁)[2], Ming-Liang Li(李明亮)[1], Guang-Jian Gao(高广健)[1], Yan-Xun Xiang(项延训)[3**]

[1]*Department of Physics, Army Logistics University of PLA, Chongqing 401331*
[2]*College of Aerospace Engineering, Key Laboratory of Optoelectronic Technology and Systems (Ministry of Education), Chongqing University, Chongqing 400044*
[3]*School of Mechanical and Power Engineering, East China University of Science and Technology, Shanghai 200237*

(Received 29 August 2018)

We analyze the effect of second-harmonic generation (SHG) of primary Lamb wave propagation in a two-layered composite plate, and then investigate the influence of interfacial properties on the said effect at low frequency. It is found that changes in the interfacial properties essentially affect the dispersion relation and then the maximum cumulative distance of the double-frequency Lamb wave generated. This will remarkably influence the efficiency of SHG. To overcome the complications arising from the inherent dispersion and multimode natures in analyzing the SHG effect of Lamb waves, the present work focuses on the analysis of the SHG effect of low-frequency dilatational Lamb wave propagation. Both the numerical analysis and finite element simulation indicate that the SHG effect of low-frequency dilatational Lamb wave propagation is found to be much more sensitive to changes in the interfacial properties than primary Lamb waves. The potential of using the SHG effect of low-frequency dilatational Lamb waves to characterize a minor change in the interfacial properties is analyzed.

PACS: 43.35.+d, 43.25.+y, 43.20.Mv DOI: 10.1088/0256-307X/35/11/114302

It is known that layered composite plates are widely used in aerospace, shipping and other industries owing to their excellent structural performance.[1−3] Generally, the interfaces of layered composite plates serve as a link of movement and a buffer against dislocation between layers to some extent.[4−6] It is known that the interface is a critical point in the process of degradation of a layered composite plate in service.[6−9] To ensure structural safety, it is of significance to develop an effective method to accurately monitor minor changes in the interfacial properties of a layered composite plate.

Based on the theoretical framework for the generation of the cumulative second harmonic of Lamb wave propagation in layered plates with imperfect interfaces, Deng *et al.* first analyzed the relationship between the efficiency of second-harmonic generation (SHG) and the interfacial properties at high frequency.[2] However, due to the complications arising from the inherent dispersion and multimode natures of Lamb waves at high frequency, it is difficult to extract the signal of pure primary wave mode whose propagation induces the generation of second harmonics increasing with the propagation distance. In comparison, the selection of Lamb waves in the low frequency region can ensure the existence of a single pure Lamb wave mode and can simplify the post processing of signals received.[10−16] However, few investigations have been carried out searching for the potential of accurately monitoring the interfacial properties of layered composite plates. Considering the advantages of both the low-frequency Lamb waves and the finite element (FE) simulation that can provide a straightforward physical insight into the process of nonlinear wave propagation without too much mathematical complexity,[10−13] the present work focuses on the analysis of the effect of SHG of low-frequency Lamb wave mode in layered composite plates.

For simplicity, only a two-layered composite plate with two solid layers is considered. The materials of the two solid layers are assumed to be isotropic and homogeneous with no attenuation and no dispersion. The coordinate system associated with the two-layered composite plate is shown in Fig. 1, where the coordinate origin is located at the interface (namely an ultrathin interfacial layer whose thickness h is much smaller than the acoustic wavelength).[5,9] It is known that the properties of the interface between the two solid layers can be characterized by the normal and the tangential interfacial stiffness constants (denoted by K_{N} and K_{T}, respectively).[8,9]

When the thickness h of the interfacial layer is much smaller than the acoustic wavelength and its mass density is negligible compared with that of the two solid layers, both K_{N} and K_{T} can be determined by[2,5,7−9]

$$K_{\mathrm{N}} = E_0(1-\nu_0)/[h(1+\nu_0)(1-2\nu_0)],$$
$$K_{\mathrm{T}} = E_0/[2h(1+\nu_0)], \quad (1)$$

where E_0 and ν_0 are the equivalent Young modulus and Poisson's ratio of the material of the ultrathin interfacial layer, respectively.[5,7−9] For a perfect interface, K_{N} and K_{T} are infinite. The degradation of the interfacial properties can be modeled by a reduction in either or both K_{N} and K_{T}.

According to the mechanical boundary conditions, the dispersion equation of Lamb wave propagation can formally be written as[2]

$$|[\boldsymbol{M}(\lambda_i, \mu_i, \rho_i, d_i, K_{\mathrm{N}}, K_{\mathrm{T}}, \omega, k_{\mathrm{p}}^{(\omega)})]|_{8\times 8} = 0, \quad (2)$$

*Supported by the National Natural Science Foundation of China under Grant Nos 11834008, 11632004, 11474361 and 11622430.
**Corresponding author. Email: dengmx65@yahoo.com; yxxiang@ecust.edu.cn
© 2018 Chinese Physical Society and IOP Publishing Ltd

where $[\boldsymbol{M}]_{8\times8}$ is the coefficient matrix of the boundary condition equation, ρ_i, λ_i and μ_i are the mass density and Lame constants of the ith layer, respectively ($i = 1$ or 2; see Fig. 1), $\omega = 2\pi f$ denotes the angular frequency, and $k^{(\omega)}$ is the corresponding wave number of the Lamb wave whose phase velocity is given by $c_{\rm p}^{(\omega)} = \omega\ /k^{(\omega)}$. Equation (2) shows that the dispersion relation is closely related with the interfacial stiffness constants $K_{\rm N}$ and $K_{\rm T}$.

According to the modal expansion approach for waveguide excitation, the second-order bulk driving forces and surface/interface stresses induced by primary Lamb wave propagation can be regarded as the excitation sources for generation of a series of double-frequency Lamb wave (DFLW) modes, whose linear superposition constitutes the total second-harmonic field (denoted by $\boldsymbol{U}^{(2\omega)}$), i.e.,[2,5]

$$\boldsymbol{U}^{(2\omega)} = \sum_m a_m(z)\boldsymbol{U}^{(2\omega,m)}(y), \tag{3}$$

where $a_m(z)$ is the expansion coefficient of the mth DFLW, and $\boldsymbol{U}^{(2\omega,m)}(y)$ is the corresponding displacement field function. Here $a_m(z)$ can be formally derived as[2,5,17–20]

$$a_m(z) = \frac{(f_m^{\rm V} + f_m^{\rm S})}{4P_{mm}} \frac{\sin(Rk^{(\omega)}z)}{Rk^{(\omega)}} \cdot \exp[jk^{(2\omega,m)}z + jRk^{(\omega)}z], \tag{4}$$

where $k^{(2\omega,m)}$ is the wave number of the mth DFLW whose phase velocity is given by $c_{\rm p}^{(2\omega,m)} = 2\omega/k^{(2\omega,m)}$, P_{mm} is the average power flow of the mth DFLW per unit width along the ox-axis, $f_m^{\rm V}$ and $f_m^{\rm S}$ are, respectively, the bulk source and surface/interface source, which originate from the second-order bulk driving forces and surface/interface stresses induced by primary Lamb wave propagation,[2,5,17–20] and $R = |c_{\rm p}^{(2\omega,m)} - c_{\rm p}^{(\omega)}|/c_{\rm p}^{(2\omega,m)}$ is used to describe the deviation of the phase velocity matching between the primary Lamb wave and the mth DFLW.[2] The maximum cumulative propagation distance (MCPD) $z_{\rm c} = \pi/[2k^{(\omega)}R]$ can be used to describe the critical distance of nonlinear cumulative effect.[12,21,22] It should be noted that Eqs. (3) and (4) are valid only within the regime of the second-order perturbation approximation.[2,5,17,20–22]

To guarantee generation of the cumulative second harmonic, the appropriate mode pair selected needs to simultaneously satisfy the phase velocity matching (i.e., $R = 0$) and non-zero power flux (i.e., $(f_m^{\rm V}+f_m^{\rm S}) \neq 0$).[2,22] When the degradation in the interfacial properties takes place, the variation in $K_{\rm N}$ and $K_{\rm T}$ will no longer guarantee the satisfaction of $R = 0$. Moreover, the value of $(f_m^{\rm V} + f_m^{\rm S})$ will change since it is inherently related to both $K_{\rm N}$ and $K_{\rm T}$.[2,5] It is expected that a minor change in $K_{\rm N}$ and $K_{\rm T}$ can sensitively influence the effect of cumulative SHG by primary Lamb wave propagation. This has been validated for high-frequency Lamb waves.[2]

Next the analysis focuses on the effect of SHG by a low-frequency Lamb wave in the layered composite plate. The materials of the upper and lower layers in Fig. 1 are aluminum (its parameters:[10,23] mass density ρ= 2700kg/m^3, longitudinal wave velocity $c_{\rm L}$=6.350 km/s, shear wave velocity $c_{\rm T}$=3.100 km/s, and third-order elastic constants l=−250 GPa, m=−333 GPa, n=−350 GPa), and their thicknesses are set to be $h_1 = 1.0$ mm and $h_2 = 0.8$ mm, respectively. According to Eq. (2), the dispersion curves of primary Lamb waves in the two-layered composite plate with a perfect interface (i.e., $K_{\rm N} = K_{\rm T}$=infinite) are shown in Fig. 2(a), and the dispersion curves of the DFLWs are computed by Eq. (2) just using $2f$ instead of f and $k^{(2\omega)}$ instead of $k^{(\omega)}$. For the case of $K_{\rm N} = K_{\rm T}$=infinite, the two-layered aluminum plate can be regarded as a single aluminum plate with a thickness of 1.8 mm (i.e., 1.0 mm+0.8 mm). When the degradation in the interface takes place, the structure of the two-layered aluminum plate is no longer exactly symmetrical with respect to the oy-axis. Consequently, the exact symmetric (S) and antisymmetric (A) Lamb waves will evolve to be the dilatational and flexural modes, respectively. Here the two types of Lamb waves in the two-layered aluminum plate are termed the dilatational and flexural modes in a general way.[23] The lowest-order dilatational/flexural modes of primary Lamb wave and DFLW at low frequency are still marked as S0/A0 and s0/a0, respectively (see Fig. 2(a)).

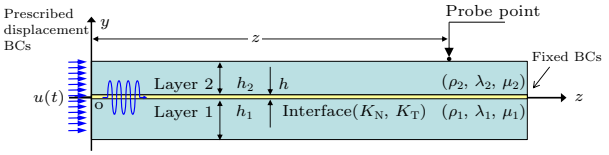

Fig. 1. Modeling of Lamb wave propagation in a two-layered composite plate.

Obviously, at low frequency (e.g., $f = 0.3$ MHz), the phase velocity matching is approximately satisfied (i.e., $c_{\rm p}^{(\omega,{\rm S0})} \approx c_{\rm p}^{(2\omega,{\rm s0})}$ or $R \approx 0$) for the mode pair determined by the points P_0 and P_0' in Fig. 2(a). When the primary S0 mode (point P_0) propagates along the oz-axis, the field of the second harmonic generated (i.e., $\boldsymbol{U}^{(2\omega)}$ in Eq. (3)) consists of the s0 and a0 modes, denoted by the intersections (i.e., P_0' and P_1').[5,12] For the case of perfect interface, the dilatational (point P_0') and flexural (point P_1') modes are exactly symmetrical and antisymmetrical, respectively, with respect to the oy-axis, and the flexural mode (point P_1') generated by propagation of the primary S0 mode (point P_0) must be zero.[2,14] Thus the second-harmonic field $\boldsymbol{U}^{(2\omega)}$ of the primary S0 mode (point P_0) is mainly dependent on the s0 mode (point P_0') due to $c_{\rm p}^{(\omega,{\rm S0})} \approx c_{\rm p}^{(2\omega,{\rm s0})}$.[12,13] Even though the degradation in the interface took place, the contribution of the a0 mode (point P_1') to $\boldsymbol{U}^{(2\omega)}$ was still negligible since the phase velocity $c_{\rm p}^{(2\omega,{\rm a0})}$ at point P_1' was quite different from $c_{\rm p}^{(\omega,{\rm S0})}$.[22]

Next we focus on analyzing the influence of the interfacial properties on the s0 mode (point P_0') generated. For convenient comparison with the subse-

quent FE simulation, the relationship $K_T/K_N = 6/31$ is assumed when the degradation of the perfect interface takes place. For several different interfacial statuses (IS; characterized by different K_N and K_T), the phase and group velocities (c_p and c_g) of the mode pair (S0−s0) at $f = 0.3$ MHz are presented in Table 1, as well as the parameters R and MCPD z_c. It is found that, when the value of K_N drops from 10^{16} N/m^3 to $10^{13.4}$ N/m^3, the relative change rate of the group velocity of the primary S0 mode is within 0.4%. In contrast, the deviation between $c_p^{(\omega,S0)}$ and $c_p^{(2\omega,s0)}$ (i.e., R) increases from 1.69% to 8.26%. The phase velocity approximate matching (i.e., $c_p^{(\omega,S0)} \approx c_p^{(2\omega,s0)}$) is no longer satisfied, which can remarkably affect the value of parameter MCPD z_c. It is noted that the calculation results under $K_N = 10^{16}$ N/m^3 are almost the same as those under K_N=infinite.

Table 1. Some parameters of the mode pair (S0 − s0) versus K_N ($K_T/K_N = 6/31$, $f = 0.3$ MHz).

Interfacial Status	logK_N (N/m^3)	$c_g^{(\omega,S0)}$ (km/s)	$c_p^{(\omega,S0)}$ (km/s)	$c_p^{(2\omega,s0)}$ (km/s)	R (%)	z_c (mm)
IS 0 (perfect)	16.0 (infinite)	5.335	5.386	5.296	1.69%	265.6
IS I	15.5	5.335	5.386	5.296	1.70%	264.6
IS Ⅱ	15.0	5.334	5.386	5.295	1.72%	261.6
IS Ⅲ	14.5	5.333	5.386	5.291	1.79%	250.6
IS Ⅳ	14.0	5.331	5.385	5.275	2.09%	214.7
IS V	13.8	5.328	5.384	5.256	2.44%	183.9
IS Ⅵ	13.6	5.323	5.383	5.209	3.34%	134.2
IS Ⅶ	13.4	5.314	5.382	4.971	8.26%	54.3

Table 2. The values of K_N and K_T for different ISs ($h = 0.01$ mm, $\nu_0 = 0.38$, $K_T/K_N = 6/31$, and $f = 0.3$ MHz).

IS	IS 0 (perfect)	IS I	IS Ⅱ	IS Ⅲ	IS Ⅳ	IS V	IS Ⅵ	IS Ⅶ
logK_N (N/m^3)	16.0	15.5	15.0	14.5	14.0	13.8	13.6	13.4
E_0 (GPa)	53.5	16.9	5.35	1.69	0.535	0.336	0.212	0.134
$c_g^{(\omega,S0)}$ (km/s) (Analytical)	5.335	5.335	5.334	5.333	5.331	5.328	5.323	5.314
$c_g^{(\omega,S0)}$ (km/s) (FE)	5.386	5.382	5.371	5.376	5.376	5.353	5.376	5.382
Relative error (%)	0.96	0.89	0.69	0.80	0.84	0.47	1.00	1.28

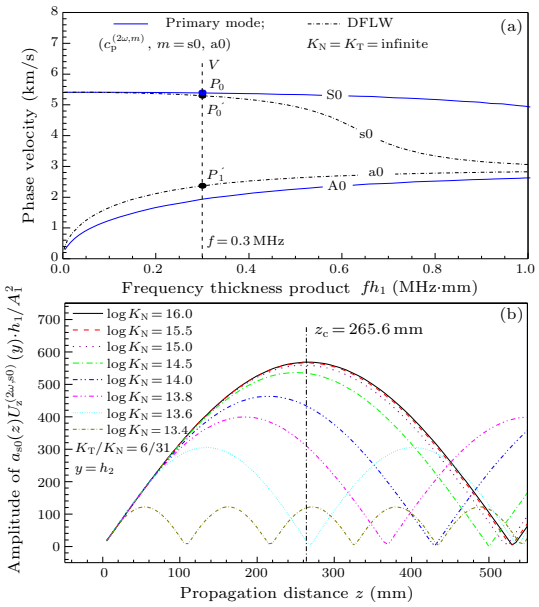

Fig. 2. (a) Dispersion curves of Lamb waves under a perfect interface. (b) Curves of amplitude of the in-plane displacement component of the s0 mode (point P_0') versus propagation distance under different K_N.

As listed in Table 1, the approximate phase velocity matching (e.g., $R = 1.69\%$) can still guarantee the generation of cumulative second harmonics within a considerable distance of propagation ($z_c = 265.6$ mm). When the values of K_N and K_T decrease as listed in Table 1, based on Eqs. (3) and (4), Fig. 2(b) shows the numerical analysis curves of the amplitude of $a_{s0}(z)U_z^{(2\omega,s0)}(y)\cdot h_1/A_1^2$ (at $y = h_2$) versus the propagation distance, where $U_z^{(2\omega,s0)}(y)$ is the in-plane displacement component of $\boldsymbol{U}^{(2\omega,s0)}(y)$, and A_1 is the amplitude of the primary S0 mode at the upper surface $y = h_2$ (see Fig. 1). Clearly, the effect of SHG of the primary S0 mode is closely related to the degradation in the interfacial properties. The amplitude of the s0 mode generated is proportional to $|\sin(Rk^{(\omega)}z)/(Rk^{(\omega)})|$ (see Eq. (4)), which is a key factor that affects the beat-effect of the second-harmonic amplitude with propagation distance.

Next, the validity of modeling and numerical analysis presented above will be further confirmed with Comsol Multiphysics®, a commercial FE software. The two-dimensional model with the prescribed displacement and fixed boundary conditions (BCs) is used for the FE simulation of the s0 mode generation by primary S0 mode under different interfacial properties (see Fig. 1). The parameters of the composite plate for the FE simulation are the same as that given in the numerical analysis presented above.

Here the interface in Fig. 1 is assumed to be a thin layer of epoxy resin with a thickness of $h = 0.01$ mm, which is far less than the wavelength of the primary S0 mode at $f = 0.3$ MHz. When the equivalent Poisson's ratio ν_0 of the epoxy resin is kept unchanged ($\nu_0 = 0.38$) while its equivalent elastic modulus E_0 decreases,[5,9] based on Eq. (1), different interfacial statuses can be obtained just through adjusting the value of E_0 (see Table 2). It should be noted that, when $\nu_0 = 0.38$ is kept unchanged, based on Eq. (1), there is a relationship between K_T and K_N, i.e., $K_T/K_N = (1 - 2\nu_0)/2(1 - \nu_0) = 6/31$.

The primary S0 mode (point P_0) at $f = 0.3$ MHz is excited by enforcing a prescribed displacement $u(t)$ (only with the tangential component) with a Hanning-

windowed sinusoidal tone-burst on the left end, which is expressed as[5,10,12]

$$u(t) = \frac{1}{2}A_0(1-\cos(2\pi ft)) \times \sin(2\pi ft/N), \quad (5)$$

where A_0 is the amplitude of the excited signal, and its value is set to be 10^{-7} m in the numerical simulation, as an amplitude of 10^{-7} m is typical for elastic wave propagation in a solid.[10] The value of cycle number N is set to be 20. In general, the maximum element size and time step should, respectively, be less than 1/20 of the wavelength and the reciprocal of the frequency of the double-frequency s0 mode (point P_0' in Fig. 2(a)).[13]

For the case of a perfect interface, the original time-domain signal of in-plane displacement (detected at $z = 240$ mm away from the excitation source) is shown in Fig. 3(a). For direct observation of the time-domain signals of the fundamental wave (0.3 MHz) and second harmonic (0.6 MHz) generated, two sets of band-pass (0.25–0.35 MHz and 0.57–0.63 MHz) digital filtering processing are, respectively, applied on the original signal given in Fig. 3(a). Hereby, the corresponding time-domain signals of the fundamental wave and the second harmonic generated are clearly shown in Figs. 3(b) and 3(c), respectively.

When the probe is located at two different positions (with a separation of Δz), the corresponding time-domain signal similar to that shown in Figs. 3(a)–3(c) can be obtained, and its group velocity can be determined by $c_g^{(\omega)} = \Delta z/\Delta t$($\Delta t$: difference of time delay). The group velocity $c_g^{(\omega)}$ via FE simulation is found to be 5.386 km/s, which is very close to the theoretical group velocity of the S0 mode ($c_g^{(\omega,\mathrm{S0})} = 5.335$ km/s) in the composite plate with a perfect interface (see Table 2). It is certain that the signal observed in Figs. 3(a)–3(c) is the S0 mode desired (point $P0$ in Fig. 2(a)). In allusion to different interfacial statuses listed in Table 2, the corresponding time-domain signal similar to that in Figs. 3(a)–3(c) and its group velocity can be obtained via FE simulation. It is found that the linear property (e.g., the relative change rate of group velocity of the primary S0 mode) does not respond obviously to the degradation in the interface.

Referring to the different interfacial statuses listed in Table 2, at a given propagation distance z, the amplitudes of the S0 mode (A_1) at 0.3 MHz and the s0 mode (A_2) at 0.6 MHz can be obtained from the time-domain signal similar to that given in Fig. 3(a) through the fast Fourier transformation (FFT). Generally, the efficiency of SHG of primary wave propagation can be quantitatively described by the relative acoustic nonlinearity parameter $\beta_\mathrm{R} = A_2/A_1^2$.[5,12] Figure 3(d) shows $\beta_\mathrm{R} = A_2/A_1^2$ versus propagation distance under different interfacial statuses. Based on the calculation results shown in Figs. 2(b) and 3(d), the MCPD z_c via numerical analysis and z_c' via FE simulation, as well as their relative errors are listed in Table 3. It is obvious that the results from the FE simulation agree well with that from the numerical analysis (RE<6%).[13] From Fig. 3(d), it is evident that, at an appropriate propagation distance (i.e., $z = 280$ mm), the relative acoustic nonlinearity parameter β_R of the s0 mode generated can monotonically and sensitively decrease with the degradation of the perfect interface, denoted by the intersections between the vertical dashed line Γ and the curves of β_R.

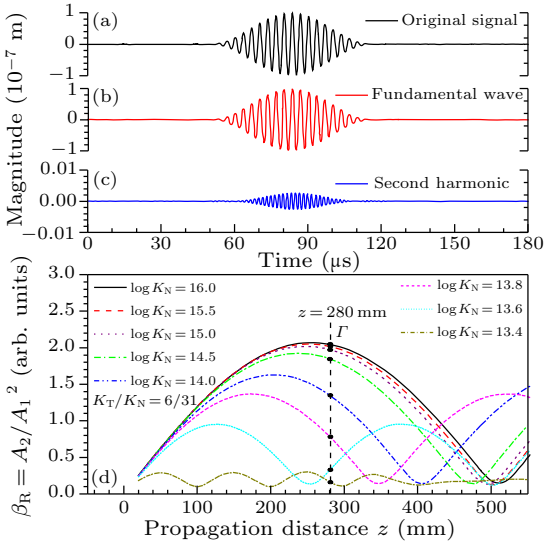

Fig. 3. (a) Original time-domain signal detected at $z = 240$ mm, and the signals of (b) the fundamental wave and (c) the second harmonic wave generated via band-pass digital filtering processing. (d) Relative nonlinearity parameter β_R versus propagation distance under different interfacial statuses at $f = 0.3$ MHz using FE simulation.

Table 3. The MCPD z_c' of the s0 mode generated and its theoretical value z_c under different ISs given in Table 2 ($K_\mathrm{T}/K_\mathrm{N} = 6/31$, $f = 0.3$ MHz).

IS	IS 0 (perfect)	IS I	IS II	IS III	IS IV	IS V	IS VI	IS VII
$\log K_\mathrm{N}$ (N/m^3)	16.0	15.5	15.0	14.5	14.0	13.8	13.6	13.4
z_c (mm) (Analytical)	265.6	264.6	261.6	250.6	214.7	183.9	134.2	54.3
z_c' (mm) (FE)	256.3	254.5	251.6	236.4	205.5	174.3	128.6	52.7
Relative error (%)	3.50	3.81	3.82	5.67	4.29	5.22	4.17	2.95

With regard to each interfacial status as listed in Table 2, the original time-domain signal detected at $z = 280$ mm, and its corresponding second-harmonic signal via a band-pass (0.57–0.63 MHz) digital filtering processing, can readily be obtained. Due to limited space, only the time-domain signals under three interfacial statuses are shown in Fig. 4, where the time-domain envelopes of fundamental wave and second harmonic (denoted by $A_{1\mathrm{f}}(t)$ and $A_{2\mathrm{f}}(t)$, respectively) are simultaneously marked by blue curves. It is found that with the decrease in K_N and K_T, the signal of the s0 mode generated gradually becomes weaker while

the original signal remains almost unchanged.

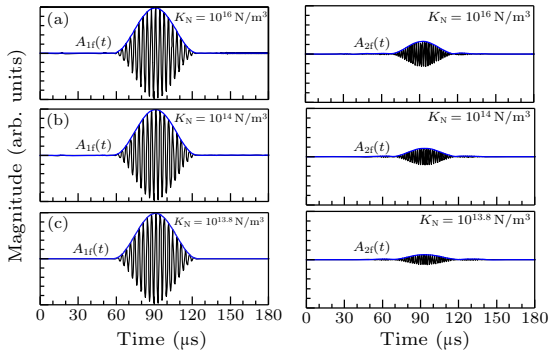

Fig. 4. The original (left) and second-harmonic (right) time-domain signals at $z = 280$ mm under three interfacial statuses: (a) $K_N = 10^{16}$ N/m^3, (b) $K_N = 10^{14}$ N/m^3, and (c) $K_N = 10^{13.8}$ N/m^3. Here $K_T/K_N = 6/31$.

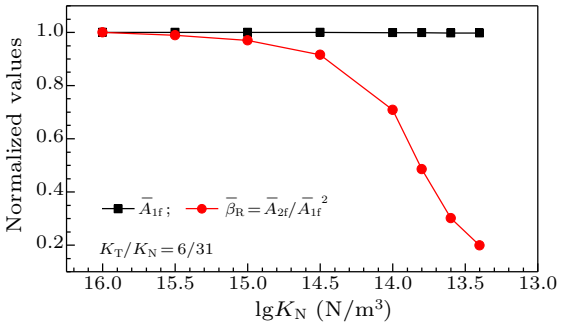

Fig. 5. Curves of normalized $\bar{A}_{1f}$ and $\bar{\beta}_R$ versus different interfacial status.

It is known that the integrated amplitudes, $\bar{A}_{1f} = \int_{t_1}^{t_2} A_{1f}(t)dt$ and $\bar{A}_{2f} = \int_{t_1}^{t_2} A_{2f}(t)dt$, can respectively be used to describe the transfer efficiency of the primary wave (S0 mode) propagation and the efficiency of SHG (s0 mode), where $A_{1f}(t)$ and $A_{2f}(t)$ are completely located between t_1 and t_2, respectively.[2,5] For the time-domain signal similar to that shown in Fig. 4, the corresponding integrated amplitudes $\bar{A}_{1f}$ and $\bar{A}_{2f}$ can be calculated for different interfacial statuses as listed in Table 2, where the integral time range is always set to be $t_1 = 0\,\mu$s and $t_2 = 180\,\mu$s. Furthermore, Fig. 5 shows the curves of normalized $\bar{A}_{1f}$ and the relative acoustic nonlinearity parameter $\bar{\beta}_R = \bar{A}_{2f}/\bar{A}_{1f}^2$ versus different interfacial statuses, where $\bar{A}_{1f}$ is kept almost unchanged while $\bar{\beta}_R = \bar{A}_{2f}/\bar{A}_{1f}^2$ exhibits a monotonic and sensitive tendency with an increase in the degradation level of interfacial properties. After degradation up to the interfacial status Ⅶ, the relative change rate of the normalized $\bar{A}_{1f}$ is within 0.3%, while the relative change rate of the normalized $\bar{\beta}_R = \bar{A}_{2f}/\bar{A}_{1f}^2$ can be as high as 80.1%. Obviously, the second harmonic decreases monotonically and sensitively at $z = 280$ mm, which is reasonably consistent with the numerical results (see Fig. 2(b)). The FE simulation results demonstrate that when a minor change in the interfacial properties (K_N and K_T) takes place, the effect of cumulative SHG by primary low-frequency S0 mode propagation can sensitively reflect a minor change in the interfacial properties.

In conclusion, the formal solution for the second harmonics of primary Lamb wave propagation in a composite plate has been obtained within a second-order perturbation approximation, and then the influence of interfacial properties on the effect of SHG was investigated. Compared with the exact phase velocity matching at high frequency, the low-frequency S0–s0 mode pair that approximately satisfies the phase velocity matching can overcome the complications arising from the inherent dispersion and multimode natures in analyzing the SHG of Lamb waves. The results of both numerical analysis and FE simulation, which agree well with each other, show that the efficiency of SHG by primary low-frequency dilatational Lamb waves can reveal a subtle change in the interfacial properties of the composite plate. Based on the use of the low-frequency dilatational Lamb wave mode pair, this work provides a promising means for sensitively assessing a minor change in the interfacial properties of layered composite plates.

References

[1] Abrate S 1991 *Appl. Mech. Rev.* **44** 155
[2] Deng M X, Wang P and Lv X F 2006 *J. Phys.* D **39** 3018
[3] Shariyat M 2009 *Compos. Struct.* **88** 228
[4] Wang Y et al 2000 *Adv. Mech.* **30** 378
[5] Li M L, Deng M X, Gao G J and Xiang Y X 2018 *J. Sound Vib.* **421** 234
[6] Davies R J and Kinloch A J 1989 *The Surface Characterisation and Adhesive Bonding of Aluminium* (Berlin: Springer) p 8
[7] Nagy P B 1992 *J. Nondestr. Eval.* **11** 127
[8] Lavrentyev A I and Rokhlin S I 1998 *Acoust. Soc. Am.* **103** 657
[9] Rokhlin S I and Wang Y J 1991 *J. Acoust. Soc. Am.* **89** 503
[10] Chillara V K and Lissenden C 2014 *Ultrasonics* **54** 1553
[11] Chillara V K and Lissenden C J 2016 *Opt. Eng.* **55** 011002
[12] Zuo P, Yu Zhou Y and Fan Z 2016 *Appl. Phys. Lett.* **109** 021902
[13] Wan X et al 2016 *Smart Mater. Struct.* **25** 045023
[14] Zhu W J, Deng M X, Xiang Y X, Xuan F Z and Liu C J 2016 *Chin. Phys. Lett.* **33** 104301
[15] Li M L et al 2016 *Chin. Phys. Lett.* **33** 124301
[16] Zuo P, Zhou Y and Fan Z 2016 *AIP Adv.* **6** 075207
[17] Deng M X 2005 *NDT E Int.* **38** 85
[18] Xiang Y X, Deng M X and Xuan F Z 2009 *J. Appl. Phys.* **106** 024902
[19] Zhu W J, Xiang Y X, Liu C J, Deng M X and Xuan F Z 2018 *J. Appl. Phys.* **123** 104902
[20] Gao G, Deng M and Li M 2015 *Acta Phys. Sin.* **64** 184303 (in Chinese)
[21] Deng M X, Wang P and Lv X F 2005 *Appl. Phys. Lett.* **86** 124104
[22] Deng M X 2003 *J. Appl. Phys.* **94** 4152
[23] Liu L P and Kaushik B 2009 *Int. J. Solids Struct.* **46** 3290